International Forum on Aeroelasticity and Structural Dynamics
IFASD 2017
25-28 June 2017, Como - Italy

# OPTIMIZATION & TESTING OF AEROELASTICALLY-TAILORED FORWARD SWEPT WINGS

**Yasser M. Meddaikar[1], Johannes K.S. Dillinger[1], and Yves Govers [1]**

[1] DLR - German Aerospace Center
Institute of Aeroelasticity
Bunsenstr. 10, 37073 Göttingen, Germany
* Muhammad.Meddaikar@DLR.de

**Keywords:** composite optimization, aeroelastic tailoring, forward swept wing

**Abstract**: Three aeroelastically-tailored forward swept wings were optimized, manufactured and tested at the subsonic SWG wind-tunnel in Göttingen. The first flexible wing was used for static tests and material characterization, the second glass-fibre reinforced wing was designed for maximizing deflection while constraining the wing tip-twist and the third carbon-fibre composite wing was designed targeting minimization of mass. The design of the wings was performed using an in-house aeroelastic optimization framework. The three wings were then tested at the SWG subsonic wind-tunnel in Göttingen.
The wind-tunnel tests for the second flexible wing were later complimented by ground-vibration tests and static load tests to evaluate its eigen frequencies, mode shapes and to measure the strains. These results are planned for use in updating the models. The work here thus presents a complete cycle of design, manufacturing and wind-tunnel testing of an optimized forward swept wing.

## 1 INTRODUCTION

Aeroelastic tailoring has been extensively studied over the last few decades and encompasses the use of beneficial tailorable properties of composites to harness or counter aeroelastic effects. The topic of composite optimization also comes into focus in this area since a composite structure with its larger design freedom in comparison with conventional metals, needs to be designed optimally in order to best harness its potential. A summary of the various composite optimization methods is provided in Ghiasi et al. [1,2]. Pertinent to the research presented here are optimization methods using lamination parameters – suitable for a stiffness-based continuous optimization; and genetic algorithms – suitable for discrete optimizations to optimize stacking sequence.

The inclusion of aeroelastic responses as part of composite optimization has been studied in the past. Shirk et al. [3] present a summary of the first works performed in the field of aeroelastic tailoring showing various trends for different applications. Vanderplaats et al. [4], for example, show that problems such as divergence in forward-swept wings and control reversal can be alleviated by tailoring composite properties without penalizing the structural weight. More recent works show the application of aeroelastic tailoring in minimizing compliance of slender wings [5], increasing flutter speed [6] and minimizing structural mass [7,8] to name a few. Dillinger et al. [9] present an efficient method for composite optimization with aeroelastic constraints using a NASTRAN-based optimization framework.

The work presented in this paper uses a forward swept wing (FSW) as the target application for aeroelastic tailoring. FSWs offer a few vital advantages over conventional swept-back

wings, for instance – increased manoeuvrability, lower induced drag, better tip-stall characteristics and the possibility of incorporating a laminar flow wing. This prompted the first investigations as early as in the 1930's itself. However, wings with a forward-sweep are inherently unstable with regards to divergence. The required increase in stiffness to counter this static instability resulted in a large increase in weight, usually outweighing the earlier mentioned benefits.

With the availability of improved materials, namely fibre-reinforced composites, a renewed interest in FSWs caught on in the mid 70's leading eventually to the development of the Grumman X-29. During its development, Krone et al. [10] showed that by tailoring composite stiffness, the critical problem of wing divergence could be alleviated. Other works [11-14] show the relative weight savings of composites over conventional metals in FSWs, the beneficial tailoring potential of composites in improving their aeroelastic performance and wind-tunnel tests conducted on tailored FSWs. At present however, these benefits do not overcome the performance offered by backward-swept wings in the field of commercial aviation. FSWs have hence been restricted to use in business jets like the HFB-320 Hansa Jet and in military applications like the KB SAT-SR10 recently in 2015.

The present work aims at applying the in-house aeroelastic tailoring framework in the design of three forward-swept wings. This is a follow-up of our earlier work presented in Meddaikar et al. [15] involving the design and wind-tunnel testing of a simple rectangular planform carbon-fibre reinforced composite wing. The present study aims to further this work by applying the developed optimization methods to the case of forward-swept wings, wherein the potential tailoring benefits of composites are more evident. For two of the three designed wings, maximization of wing deflection was chosen as the design objective. For the third wing, a conventional design objective of mass minimization was chosen. The aim of this study was firstly, to test the aeroelastic optimization framework by applying it in the design of forward swept wings and comparing results from the simulations with actual wind-tunnel tests and secondly, to demonstrate a high-flexible forward-swept wing without the nose-up twist behaviour inherent to such wings. The focus of the work was on the second highly flexible wing. For this wing, in addition to wind-tunnel tests, ground vibration tests (GVT) and static load tests were performed. The data from these is to be used in future model-updating tasks.

The first initial analysis of wind-tunnel data had been presented earlier in Ritter et al. [16] comparing in detail different aeroelastic routines developed: linear and non-linear finite element methods coupled with different linear and non-linear aerodynamic models.

The paper is outlined as follows: an overview of the aeroelastic tailoring framework is first presented along with the optimization process for the three wings; a brief explanation of the manufacturing process and the wind-tunnel test setup is presented; this is followed by results from the static tests in the wind-tunnel, outlook for future tasks and a conclusion of the work presented.

## 2 COMPOSITE OPTIMIZATION FRAMEWORK

The composite optimization framework is based on a two-step approach proposed by Ijsselmuiden et al. [17,18].

*Continuous optimization*
In the first step, a gradient-based optimization with lamination parameters (LP) as the design variables is performed. Lamination parameters [19,20] are a set of 12 variables (8 in the case of symmetric laminates) that encompass the entire stiffness information of a composite laminate. Since LPs are continuous variables, they enable the use of efficient gradient-based optimizers. Additionally, LPs are not constrained by ply angles or thickness, as a result of which the obtained design represents the theoretical upper-bound in performance that can be achieved for the given material and loading. The obtained design is used as a starting point for the next stacking sequence optimization step with the rationale being that the optimal stacking sequence design should be in the nearby vicinity in stiffness-space, to the optimal stiffness-based design.

For the optimization, the gradient-based optimizer ALDO [17] developed at the Technical University of Delft was used and this step is detailed in Dillinger et al. [9].

*Stacking sequence optimization*
The second step in the optimization framework optimizes the stacking sequence necessary for manufacturing. This is performed using a genetic algorithm (GA) incorporating a technique known as stacking sequence tables (SST – [20]). Details of the optimization tool are presented in Meddaikar et al. [22].

The optimization using SSTs ensures that the design follows the rules of laminate blending [23], thereby ensuring continuity of fibres between adjacent plies. This is necessary to guarantee manufacturability and structural integrity by preventing discontinuous plies. The approach using SSTs also provides ply-drop information between adjacent design regions, aiding in manufacturing.

*Successive structural approximations*
During an optimization, a large number of designs have to be analysed before reaching an optimum. This for practical structural problems means an expensive finite element (FE) analysis for every design evaluated. This can be computationally exhaustive depending on the complexity of the model. In order to reduce the number of required analyses, the successive structural approximation [24] approach is used. An actual structural response (for instance, stress) is replaced by an approximation of the response. Using these approximated responses, an optimal design is found and a new set of approximations is constructed at the obtained optimal point. This optimization and design-update sequence is iteratively performed until convergence. The result is that with a much reduced number of FE analyses and performing the optimization on approximations of the responses, the computational costs are greatly reduced.

The approximation $\tilde{f}$ of a response $f$ (for instance, stress in a panel i) is expressed as:

$$\tilde{f}_i = \sum_{j=1}^{N} \left( \boldsymbol{\Psi}_j^m \big|_0 : \boldsymbol{A}_j + \boldsymbol{\Psi}_j^b \big|_0 : \boldsymbol{D}_j + \boldsymbol{\Phi}_j^m \big|_0 : \boldsymbol{A}_j^{-1} + \boldsymbol{\Phi}_j^b \big|_0 : \boldsymbol{D}_j^{-1} + \alpha_j \big|_0 h_j \right) + C_0 \qquad (1)$$

The approximation is expressed in terms of the in-plane stiffness matrix $\boldsymbol{A}$, the bending stiffness matrix $\boldsymbol{D}$, their inverses and the laminate thickness $h$. The structure is divided into N design fields, each design field capable of having a different stacking sequence or effectively, a different stiffness. The linear $\boldsymbol{\Psi}$ and reciprocal $\boldsymbol{\Phi}$ sensitivity terms are calculated from a NASTRAN sensitivity analysis. The superscripts *m* and *b* denote the membrane and bending related terms respectively.

The response $f$ can be any structural response, for instance, stress in a given panel. The summation involving sensitivity terms from all the design fields, accounts also for load redistribution due to stiffness change. The sensitivity with respect to thickness $\alpha$ is included in the expression making it possible to also have mass as a response using the same approximation scheme. In the case of mass response, the sensitivity terms $\boldsymbol{\Psi}$ and $\boldsymbol{\phi}$ have zero values. The ':' operator is the matrix or Frobenius inner product. These approximations are developed based on those presented in Ijsselmuiden et al. [17].

In Equation (1), the approximations are expressed directly in terms of the stiffness matrices **A** and **D** respectively. These **A** and **D** matrices can be expressed either in terms of lamination parameters or in terms of ply layup, rendering the same approximation suitable for use either in the first lamination-parameter based continuous optimization step, or in the second stacking-sequence discrete optimization step.

The following structural and aeroelastic responses are used in the optimization.

i) Strength:

$$\widetilde{f_i} \approx \boldsymbol{\Psi}_i^m : \boldsymbol{A}_i + \boldsymbol{\Phi}_i^m : \boldsymbol{A}_i^{-1} + s_i^t \Delta N_i \tag{2}$$

ii) Buckling:

$$\widetilde{r_i} \approx \boldsymbol{\Phi}_i^b : \boldsymbol{D}_i^{-1} + s_i^t \Delta N_i \tag{3}$$

iii) Deflection:

$$\tilde{\delta} \approx \sum_{i=1}^{N} \left( \boldsymbol{\Psi}_i^m : \boldsymbol{A}_i + \boldsymbol{\Psi}_i^b : \boldsymbol{D}_i + \boldsymbol{\Phi}_i^m : \boldsymbol{A}_i^{-1} + \boldsymbol{\Phi}_i^b : \boldsymbol{D}_i^{-1} + \alpha_i h_i \right) \tag{4}$$

iv) Twist:

$$\tilde{\theta} \approx \sum_{i=1}^{N} \left( \boldsymbol{\Psi}_i^m : \boldsymbol{A}_i + \boldsymbol{\Psi}_i^b : \boldsymbol{D}_i + \boldsymbol{\Phi}_i^m : \boldsymbol{A}_i^{-1} + \boldsymbol{\Phi}_i^b : \boldsymbol{D}_i^{-1} + \alpha_i h_i \right) \tag{5}$$

Equations (2) and (3) are of the same form as Equation (1) except that for convenience's sake, the approximation is split into two parts – contribution from the change in stiffness in the panel whose response is being evaluated itself and contribution due to load re-distribution in the last term. The construction of these responses is detailed in Dillinger et al. [9].

## 3 WING DESIGN

The wing planform was chosen with a forward sweep angle of 15°, a wing half-span of 1.6*m*, root and tip chord of 0.36*m* and 0.12*m* respectively and thus a full wing aspect ratio of 13.33. A custom unsymmetrical airfoil was chosen. The entire wing was designed having five design fields each in the upper and lower skin. As mentioned earlier, each design field is defined as a region having constant stiffness properties, effectively constant laminate stacking sequence. The laminates in the five design fields were designed following rules of blending to ensure manufacturability and structural integrity. The geometry of the wing and the distribution of the design fields is shown in Figure 1.

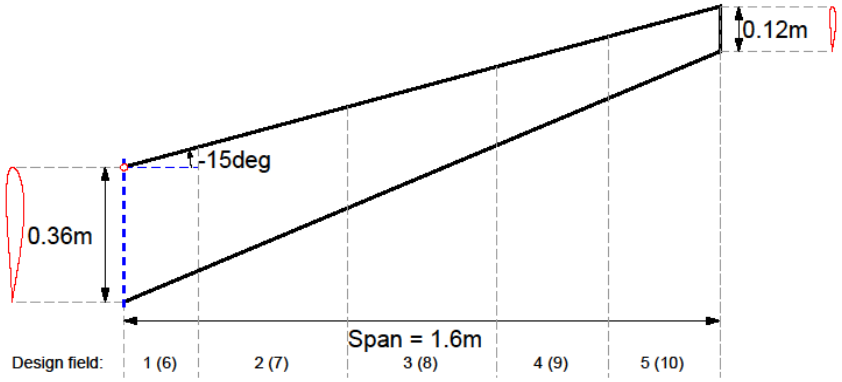


Figure 1: Wing planform showing distribution of the design fields in the skins (within brackets are the design field numbering in the lower skin)

*Load cases considered*

The wings were optimized for a sizing load case: angle of attack $\alpha = \pm 10°$ and velocity v = 60m/s. This allowed a sufficient margin of safety to the most severe wind tunnel test case: $\alpha = \pm 10°$ and v = 50m/s. These load cases are summarized in Table 1. Additionally, a knock down factor of 1.5 was applied on the material strain allowables listed Table 4.

| | Sizing in optimization | | Wind-tunnel test | |
|---|---|---|---|---|
| Load case | 1 | 2 | 3 | 4 |
| Speed (m/s) | 60 | 60 | 50 | 50 |
| Angle of attack (°) | -10° | 10° | -10° | 10° |

Table 1: Load cases – wind tunnel experiment and sizing

*Design guidelines*

The stacking sequence optimization includes the following industry-established design guidelines:

i) laminate guidelines: symmetry, balance, maximum ply contiguity set to 4, maximum ply disorientation of 45° between successive plies, +-45° plies on the outer surface for damage tolerance, 10%-rule

ii) ply-drop guidelines: outer/inner-most plies cover the entire wing, internal continuity with one continuous ply for every three dropped ones, ply drops alternatively close to and far from the laminate mid-surface

iii) global guidelines: the laminates in the design regions are blended following the definition of generalized blending

Given the relatively low number of plies required under the given loading, all laminate guidelines were dropped in the design of the three wings. An exception was the 10% rule in the case of the third mass-minimized wing in order to best represent an industrial case. Also, the ply-drop guideline requiring a continuous ply for three dropped plies was relaxed.
Unbalanced laminates were allowed in the case of all three wings.

*Evaluation of constraints*

In order to evaluate the strength constraint in the optimization, a Tsai-Wu based strain failure envelope [25] with prescribed maximum critical strains was used. The 10% rule was

implemented as a limit on the ratio between the maximum and minimum laminate stiffness [26]. The twist and deformation responses were calculated directly from their respective approximations (Equations (4), (5)).

To tackle failure due to buckling, either a large number of spars and ribs would have been required thus complicating the construction or very thick skins would have been necessary. Instead, a foam core was used in the hollow between the upper and lower skins and the wings were checked against buckling in NASTRAN, proving to be buckling-safe. The foam material used was Styrodur 3035CS.

### 3.1 Wings 1 and 2 – tip deformation maximization

Wings 1 and 2 were optimized for a design objective of deformation-maximization. Material failure was included as an optimization constraint. With the well-known wash-in problem in such a forward swept wing, an additional upper limit on the tip twist was imposed in the optimization, $\theta_{tip} < 0°$. A glass-fibre material was used in this case on account of its lower stiffness. The material properties are listed in Table 4.

Wing 1 was initially tested with static loads in a test bench to check the assumptions in the material allowables used. For these static tests (Figure 12), loads distributed at four sections simulating the aeroelastic loads were introduced. With the experience gained from the manufacturing and confidence from the static tests, Wing 2 was designed to be even more flexible with the minimum number of plies allowed in the laminates set to 1.

The SST corresponding to the optimized design of Wing 2 is shown Table 2. An SST lists all possible ply layups of blended laminates containing different number of plies. Knowing the number of plies in each of the design fields, the laminate in that design field can be read out. Figure 2 and Figure 3 show a polar distribution of the stiffness $E_1$of the laminate (($E_1(\theta) = 1/A_{11}^{-1}(\theta)$ )). The ply angles are defined with respect to a reference – the line joining the mid-points of the root and tip chords – and are considered positive when rotated in the anti-clockwise direction. Since the upper and lower skins in the case of all three wings were manufactured separately and then joined together, ensuring continuity between the fibres in the upper and lower skins was unnecessary. As a result, the two skins were characterized by their independent SSTs.

With the objective of the optimization being to maximize deformation, it is seen that the resulting design has its stiffness directed primarily away from the span, thus reducing its bending stiffness. Another interesting feature is that the stiffness is directed forward with respect to the reference. For a wing undergoing bending deformation, the net result is that a nose-down twist is generated when the wing bends upwards, thus countering the wash-in experienced in the forward swept wing.

The thickness distribution in Wing 2 is shown in Figure 4. As can be expected, it is seen that junctions near ply-drops are regions having critical strain failure indices, as shown in Figure 5. Figure 6 shows the Double Lattice Method (DLM) forces and Figure 7 the wing deformation corresponding to the final optimized design of Wing 2, obtained from a NASTRAN aeroelastic analysis.

| No. of plies | $N_{min}$ | | | | | $N_{max}$ | $N_{min}$ | | | | | $N_{max}$ |
|---|---|---|---|---|---|---|---|---|---|---|---|---|
| | 2 | | | 4 | | 6 | 2 | | | 4 | | 6 |
| | 30 | 30 | 30 | 30 | 30 | 30 | | 30 | 30 | 30 | 30 | 30 |
| | | | -75 | -75 | -75 | -75 | | | | | 0 | 0 |
| | | | | | 60 | 60 | | | 90 | 90 | 90 | 90 |
| | | | | | | 60 | | | | 90 | 90 | 90 |
| | | | | -75 | -75 | -75 | | | | | | 0 |
| | | 30 | 30 | 30 | 30 | 30 | 30 | 30 | 30 | 30 | 30 | 30 |
| Design field | **4, 5** | **3** | **2** | **1** | | | **4, 5** | **3** | **1, 2** | | | |

Table 2: SST and ply layup corresponding to Wing 2 (the last row denotes the design fields having the ply layup in that particular column)

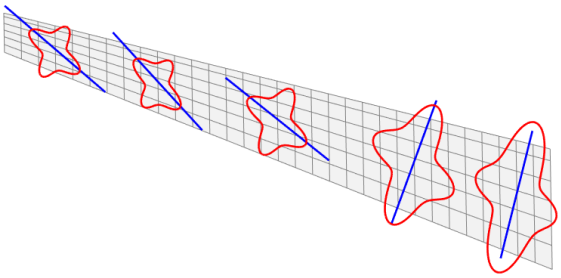

Figure 2: Wing 2 - polar stiffness ($E_1(\theta)$) – lower skin

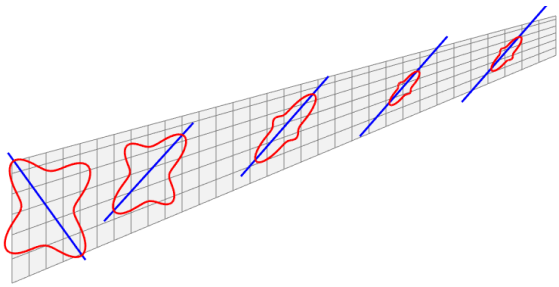

Figure 3: Wing 2 – polar stiffness ($E_1(\theta)$) – upper skin

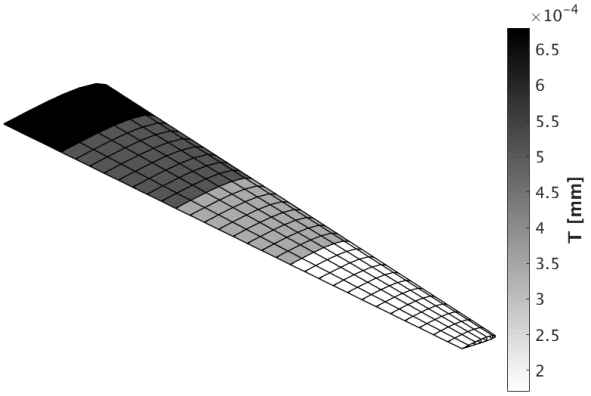


Figure 4: Wing 2 – thickness distribution

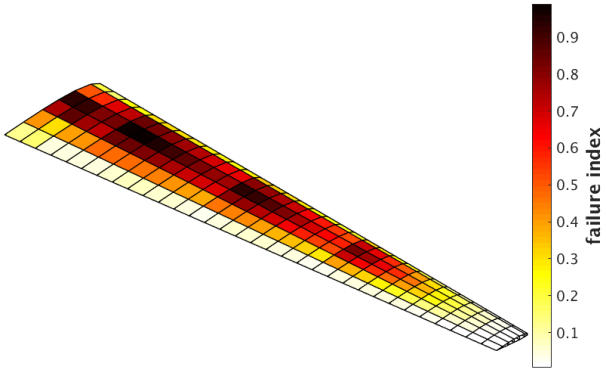


Figure 5: Wing 2- strain failure indices

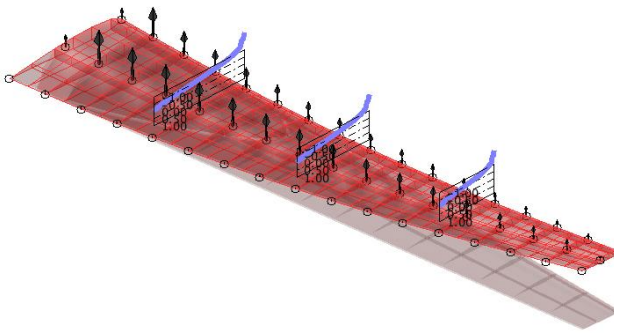

Figure 6: Wing 2 – DLM forces and $C_p$ for $\alpha = 10^o$, v = 50m/s

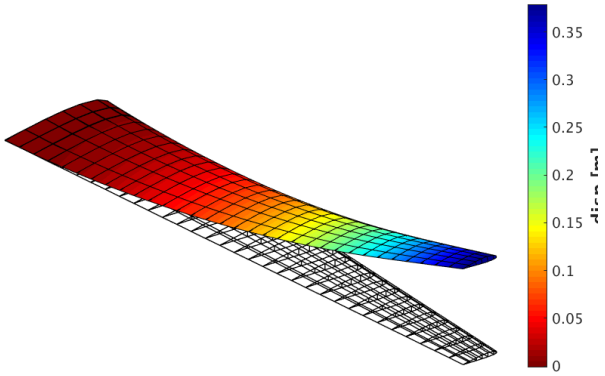


Figure 7: Wing 2 – FE (NASTRAN SOL 144) deformation for $\alpha = 10^o$, v = 50m/s

### 3.2 Wing 3 – mass minimization

The optimization-objective of Wing 3 was a conventional mass-minimization, in order to best represent an industrial case. The constraints included were strain and wing static divergence.

Carbon-fibre was chosen as the material for manufacturing in Wing 3. The SST and the ply layups of the design fields in Wing 3 are shown in Table 3, along with a polar distribution of the stiffness ($E_1(\theta)$) in Figure 8 and Figure 9. The optimization resulted in a wing having a 5-ply laminate across all the design fields in each skin. This was as a result of the design guidelines implemented, most severely the 10%-rule ensuring a minimum stiffness of the laminate in all directions. The resulting wing hence had a large safety margin in terms of the material strain constraint, as shown in Figure 10.

| | $N_{min}$ | | | | $N_{max}$ | $N_{min}$ | | | | $N_{max}$ |
|---|---|---|---|---|---|---|---|---|---|---|
| No. of plies | *4* | | *6* | | *8* | *4* | | *6* | | *8* |
| | 15 | 15 | 15 | 15 | 15 | 0 | 0 | 0 | 0 | 0 |
| | -15 | -15 | -15 | -15 | -15 | 30 | 30 | 30 | 30 | 30 |
| | | 90 | 90 | 90 | 90 | | -75 | -75 | -75 | -75 |
| | | | | 60 | 60 | | | | -15 | -15 |
| | | | | | 60 | | | | | -15 |
| | | | 90 | 90 | 90 | | | -75 | -75 | -75 |
| | -15 | -15 | -15 | -15 | -15 | 30 | 30 | 30 | 30 | 30 |
| | 15 | 15 | 15 | 15 | 15 | 0 | 0 | 0 | 0 | 0 |
| Design field | | **1 - 5** | | | | | **1 - 5** | | | |

Table 3: SST and ply layup corresponding to Wing 3 (the last row denotes the design fields having the ply layup in that particular column)

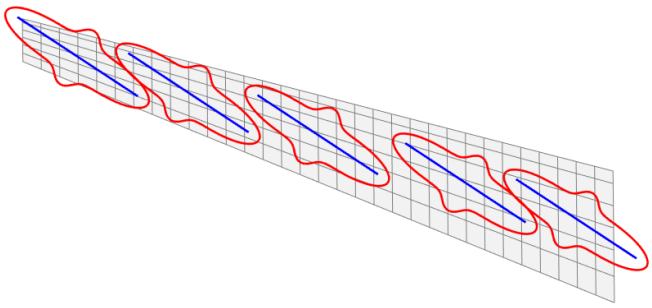

Figure 8: Wing 3 – polar stiffness ($E_1(\theta)$) – lower skin

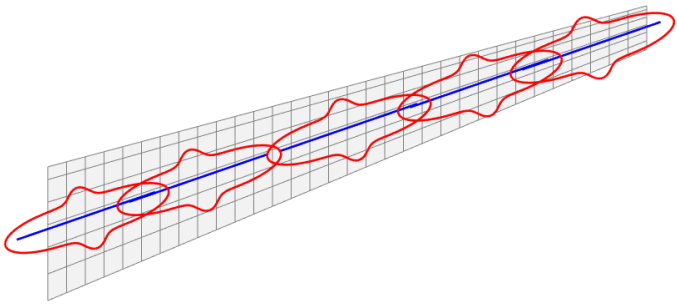

Figure 9: Wing 3 – polar stiffness ($E_1(\theta)$) – upper skin

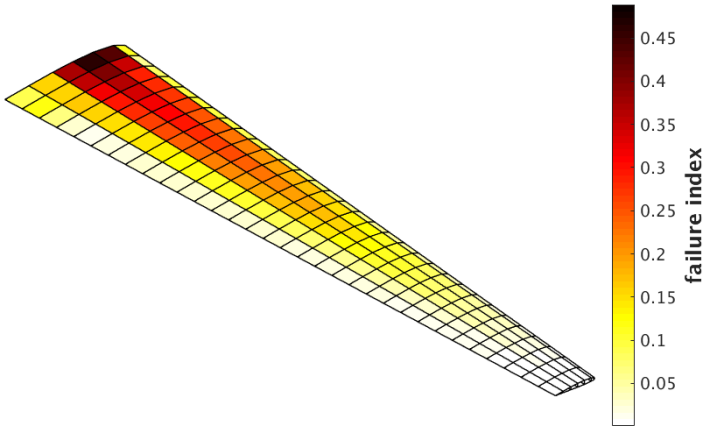


Figure 10: Wing 3 – strain failure indices

## 4 WING MANUFACTURING

The wing halves (upper and lower skin) were manufactured in two moulds separately after hand laying-up of the plies, vacuum-bagging and curing them at room temperature. After this, the two halves were joined together. Two spars running at one-thirds and two-thirds of the chord were included in the wing to help effectively transfer the loads to the wing root. Additionally, a 'foot' with a rectangular cross-section comprising of wood re-enforced with carbon fibre fabric extended from the first design field to 20cm outside the wing, as shown in Figure 11. The wing was clamped for the wind-tunnel tests at this foot, which formed an inherent part of the wing structure itself. This ensured that during wind-tunnel experiments, the free play between the wing and clamp was kept to a minimum, a problem that had been encountered during a previous set of experiments when the clamp was placed directly on the wing at the root section.

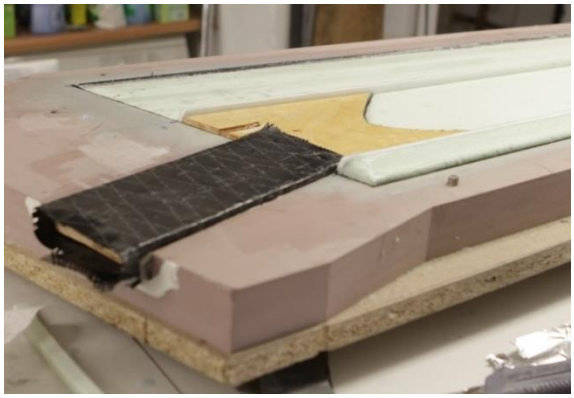

Figure 11: Adaptation of wing root for clamping

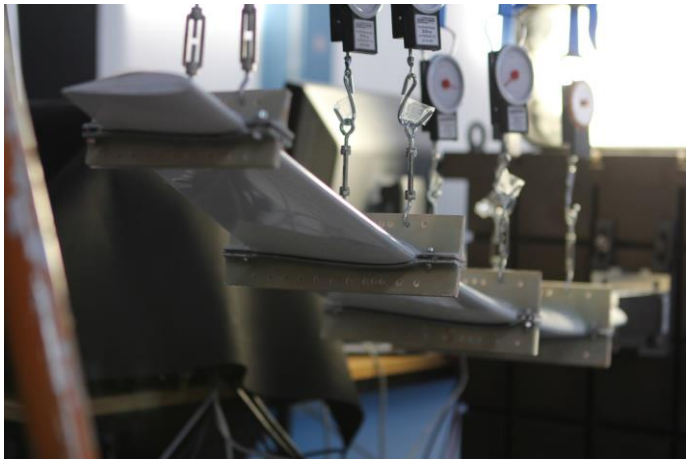

Figure 12: Static tests on Wing-1

In the case of Wing 3, a UD carbon fibre T700 material impregnated with epoxy resin was used. While in the case of Wings 1 and 2, an E-Glass fabric with a majority of fibres (93%) in the weft direction was used in the manufacturing. Wing 2 was additionally fabricated with an optic strain measurement fibre running span-wise at the quarter-chord position, capable of measuring strains with a very fine resolution.

| | E-Glass 93/7* Epoxy | T300 UD Epoxy |
|---|---|---|
| $E_1$ (GPa) | 36.75 | 104.98 |
| $E_2$ (GPa) | 12.25 | 8.35 |
| $G_{12}$ (GPa) | 3.95 | 3.37 |
| $\nu_{12}$ | 0.23 | 0.275 |
| th (mm) | 0.17 | 0.0889 |
| $\rho$ (kg/m³) | 2550 | 1500 |
| $[\epsilon_t, \epsilon_c, \gamma]$ | [3.3, 2.2, 2.2] % | [1.5, 1.1, 2.0] % |
| knock-down factor on strain limits | 1.5 | 1.5 |

Table 4: Material properties

* calculated from classical laminate theory, with properties of E-Glass Silenka

## 5 WIND-TUNNEL TESTING

The wings were tested at the subsonic Side Wind Tunnel Test Facility (SWG) in Göttingen. The wind-tunnel is a closed-circuit subsonic tunnel with a maximum velocity of 60m/s and a test section having cross-sectional dimensions 2.4m x 1.6m. The wings were tested at velocities from 10 to 50m/s in steps of 10m/s and at angles of attack $\alpha = -10°$ to 10° in steps of 1° for static measurements. For the dynamic case, a sinusoidal excitation was provided with the pitching oscillator for different combinations of reduced frequencies between k = 0.07 and 1.0, amplitude of oscillation between $\theta_a$ = 1° and 4° and velocities between 10m/s and 50m/s.

*Piezoelectric balance*

The wing was mounted on to a six-component piezoelectric balance [27] through a clamp. The root forces in the vertical, horizontal and span-wise directions and the moments about the three axes were measured using the balance.

*Pitching oscillator*

The wing through the clamp and balance was mounted on to a pitching oscillator, shown in Figure 13. The angle of attack of the wing in the case of static tests and pitching motion for the dynamic tests were controlled using the oscillator.

*Deformation measurement*

A marker-based image correlation system was used to measure the deformation at distinct points of the wing. A total of 32 markers (shown in Figure 14) were placed on the wing upper skin and these were tracked by the measurement system. The system comprised of two Microtron 1310 CCD video cameras and a 3D image correlation system picCOLOR. Knowing the positions of the markers in the wind-off state and the tracked markers after wind-on, the deflection and twists could be calculated.

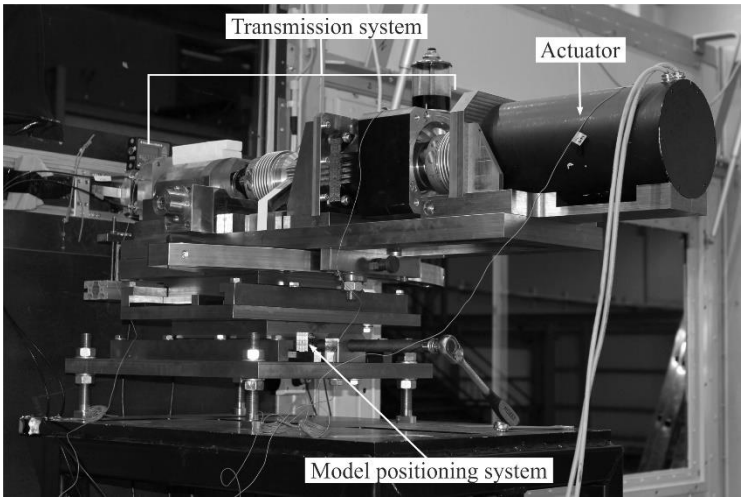


Figure 13: Wind-tunnel test setup (outside)

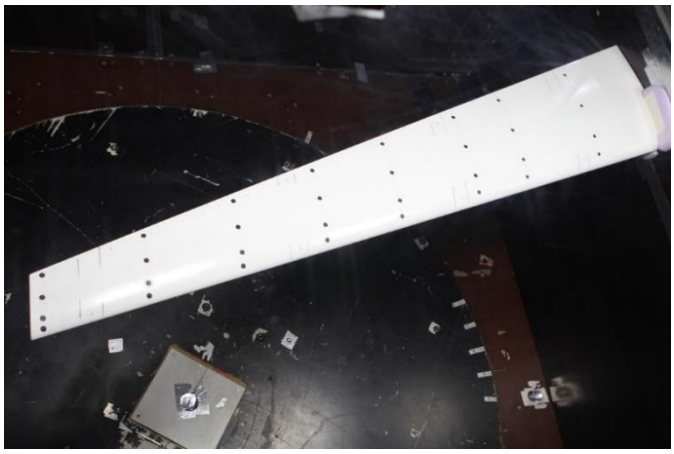

Figure 14: Wing and markers for position measurement

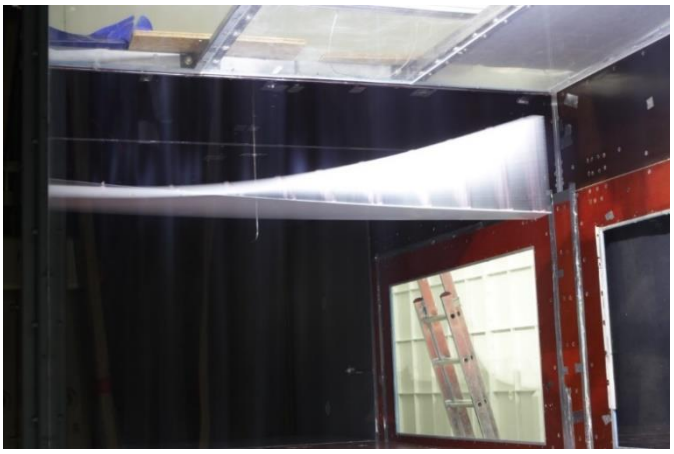

Figure 15: Blended image showing deformation of Wing 2, at v = 50m/s, $\alpha = 0^o$ through $10^o$

## 6 WIND-TUNNEL TEST RESULTS

The data from the wind tunnel measurements comprised of forces and moments from the piezoelectric balance and the marker positions obtained from the image correlation system. The deformation was then calculated at the discrete marker points from the difference in marker position at wind-on and wind-off conditions.

The aim of Wing-2 was to demonstrate a flexible wing with a maximum displacement of at least 15% of the wing semi-span. Figure 15 shows a blended image with the deformation of Wing 2 at 50m/s, through angles of attack $\alpha$ from $0^o$ to $10^o$.

The maximum displacement obtained at a velocity of 50m/s and angle of attack $10^o$ was 18.4% of the wing sem-span and is shown in a comparison between wind-tunnel results (WT) and simulation results (FE) in Figure 16. The FE results shown in this paper are from a NASTRAN SOL144 aeroelastic analysis.

Before a deeper analysis of the results, it is noteworthy to consider the following two points:

- the tests for velocity = 50m/s represent some uncertainties. At very high displacements (>15%), the wing itself was in close proximity to the upper wall of the wind-tunnel, possible causing interference effects. Secondly, the tunnel at 50m/s tended to heat quite quickly on account of the the friction in the wind-tunnel leading to a possible softening of the wing at these measurement points. For these reasons, the results presented further are restricted to velocities up to 40m/s.
- Figure 17 shows a time-history of the lift measured using the piezo-balance at different angles of attack for a velocity of 40m/s. It is seen that until an angle of attack of $7^o$ the time-history is steady and the values of lift are nearly equally placed for incremental angles of attack. Beyond $7^o$, the lift force for the static measurement points become quite unsteady. A possible reason for this is due to flow separation occuring at higher angles of attack. This is also visible for higher negative angles of attack. Consequently, the results presented below are restricted to cases within angles of attack = $\pm 7^o$ except when explained.

The FE simulations presented here have been corrected for the density changes arising from the variation in temperature in the wind-tunnel.

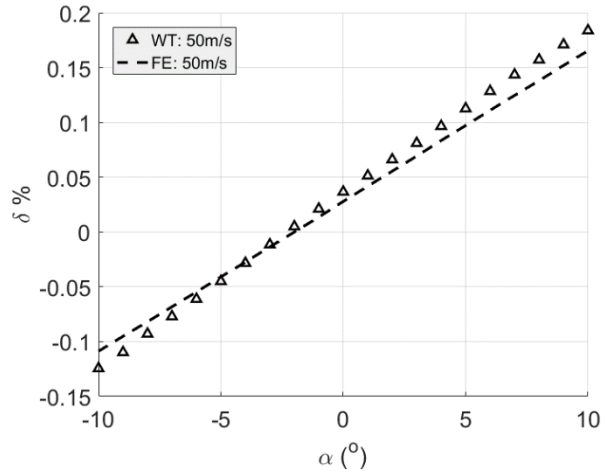


Figure 16: Displacement (% with respect to semi-span) vs angle of attack for velocity v = 50m/s

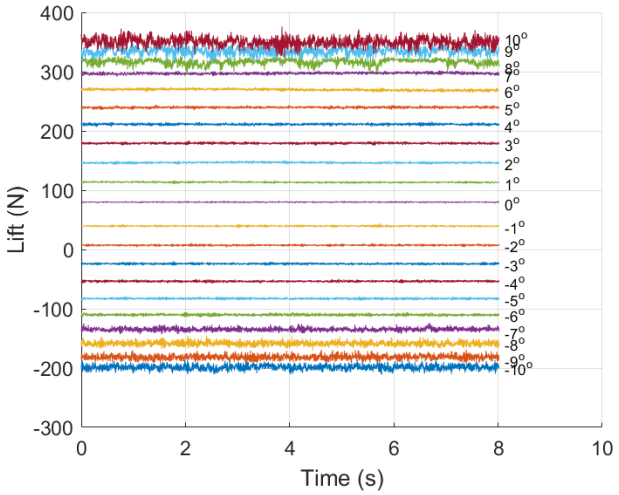


Figure 17: Lift over duration of measurement for different angle of attack at velocity v = 40m/s

### 6.1 Wing deformation

The displacement for different velocities is plotted against angle of attack in Figure 18 showing a linear behavior as expected. The exception is at higher angles of attack due to the reasons mentioned before, namely unsteady and reduced aerodynamic lift. The figure shows a good correlation between the wind-tunnel results and the FE simulations with the largest deviation of ~8% at 40m/s. With deformation being proportional to lift and lift in turn being proportional to the dynamic pressure, Figure 19 shows an expected linear relation between deformation and dynamic pressure.

The wing-twist was calculated knowing the marker position at two markers in a given chord-section. A span-wise distribution of the wing-twist is shown in Figure 20 for different angles of attack. For such small twist values, the difference in displacements at two chord sections required to calculate the twist is so small, that it is within the accuracy of the measurement system itself. Of importance is that the tip twist is always close to 0°, which was chosen as a requirement for the demonstration of aeroelastic tailoring in the forward-swept flexible wing.

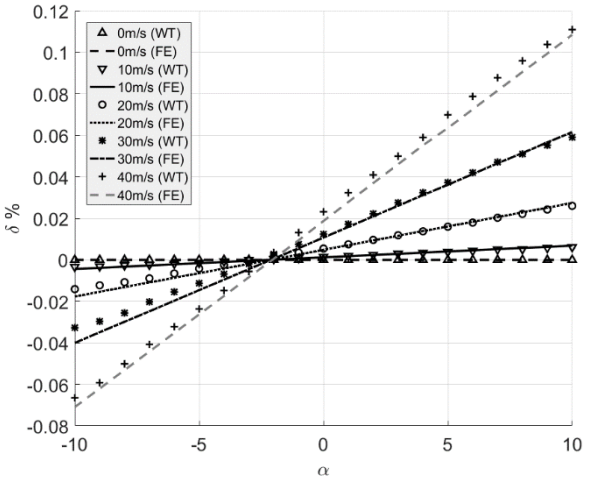


Figure 18: Displacement (% with respect to semi-span) vs angle of attack for different velocities

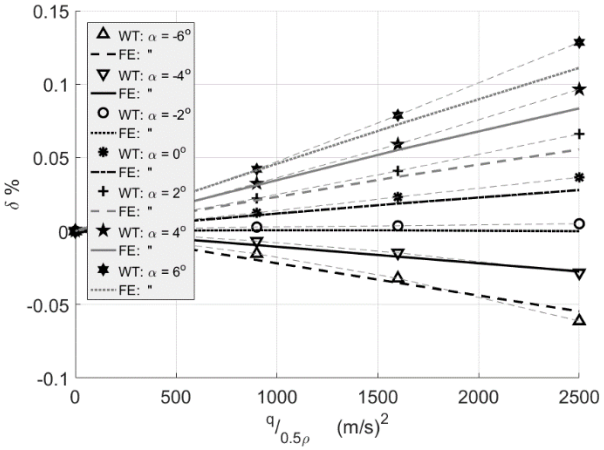


Figure 19: Displacement (% with respect to semi-span) vs dynamic pressure (divided by 0.5*density) for different angles of attack

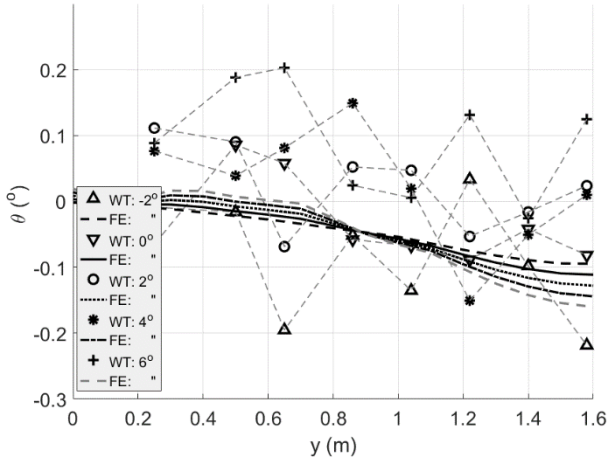


Figure 20: Wing-twist along span for different angles of attack at velocity v = 30m/s

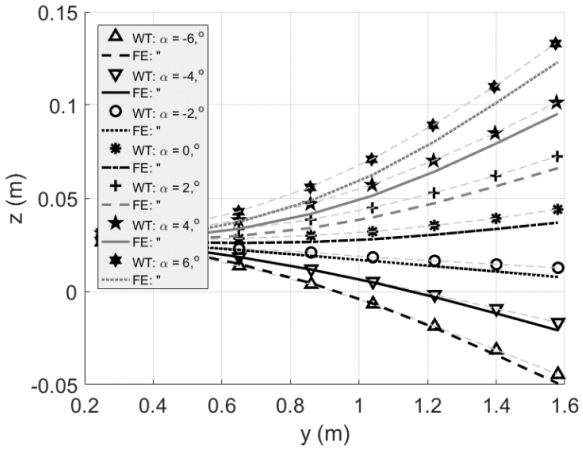


Figure 21: Span-wise displacement for different angles of attack, velocity v = 40m/s

### 6.2 Wing lift

The forces and moments were measured using the piezoelectric balance. Using the forces normal and parallel to the axis of the balance along with the measured angle of attack, the measured lift was calculated. Shown in Figure 22 is a variation of the lift with the angle of attack. The figure shows a good correlation between the measured and simulated results with a maximum deviation in the 40m/s case of ~5.6% until an angle of attack of 7º. Beyond this, the lift force drops for all velocity cases, further strenghtening the reasoning mentioned earlier – due to flow separation.

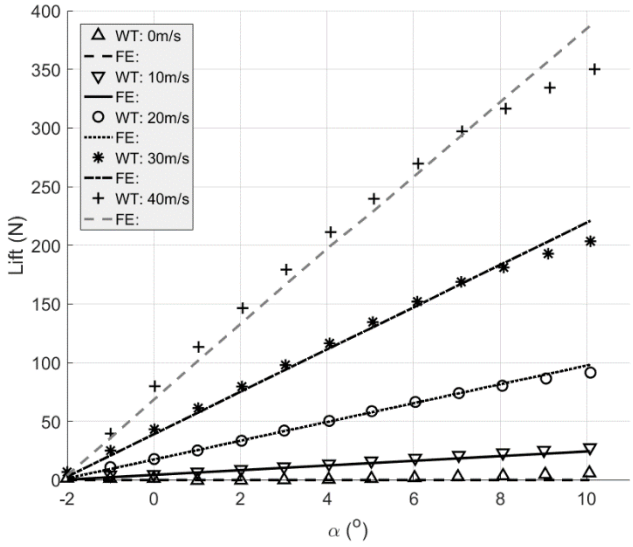


Figure 22: Lift vs angle of attack for different velocities

## 7 OUTLOOK – GVT DATA AND STRAIN MEASUREMENT

During any design process, a deviation in the simulation and experimental results is foreseeable due to limitations in the fidelity of a model useable in an optimization and importantly, due to manufacturing deviations. One possible method to improve the simulation FE models to better match the actual manufactured structure is via a model-updating step using a reliable test set-up.

As part of this work, a ground vibration test (GVT) was performed on the wing using a shaker as an excitation source and a Laser Doppler vibrometer (LDV) as the measurement technique, with a high resolution of measurement points. Since the LDV allows measurement of displacement or velocity in a single direction (out-of-plane in this case), 10 accelerometers were placed at the leading edge of the wing to capture the in-plane modes as well. The combined out-of-plane data from the laser vibrometer and in-plane acceleration data from the accelerometers were then used for the modal analysis of the measured time-data.

The eigen frequencies and the mode shapes of Wing 2 obtained from the processed time-data are presented Table 5 and Figure 23 respectively.

| *GVT* | *NASTRAN SOL103* | *Mode type* |
|---|---|---|
| 10.48 | 12.75 | 1st bending |
| 35.86 | 40.54 | 2nd bending |
| 83.74 | 93.59 | 3rd bending |

Table 5: Comparison of eigen frequencies (Hz) – GVT vs FE

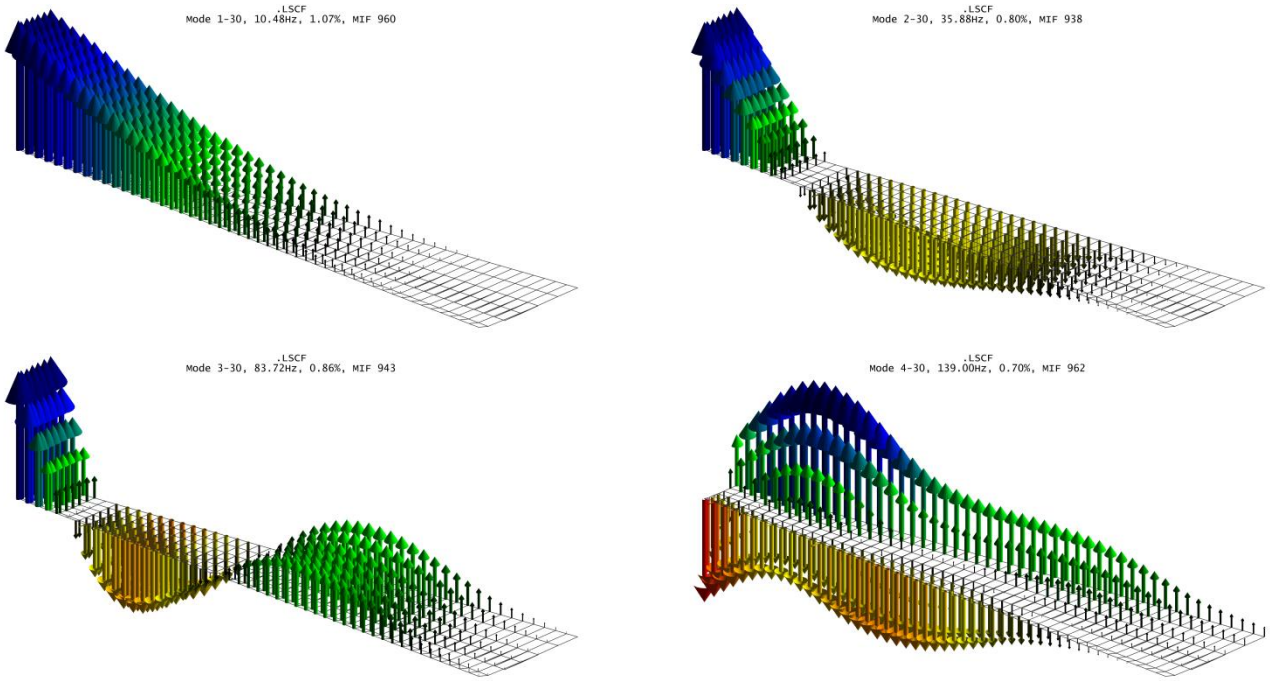


Figure 23: Mode shapes 1-4 of Wing 2 obtained from measurements using the Laser vibrometer system

In order to better compare and validate the strain data, static tests were performed on Wing 2 and the installed optical strain measurement fiber was used to extract the strain data. Figure 24 for example shows the span-wise strain data when bending loads were introduced in steps at a location of 1.1m along the span. The regions experiencing a sharp jump in strain values are a result of the ply-drop present in those regions.

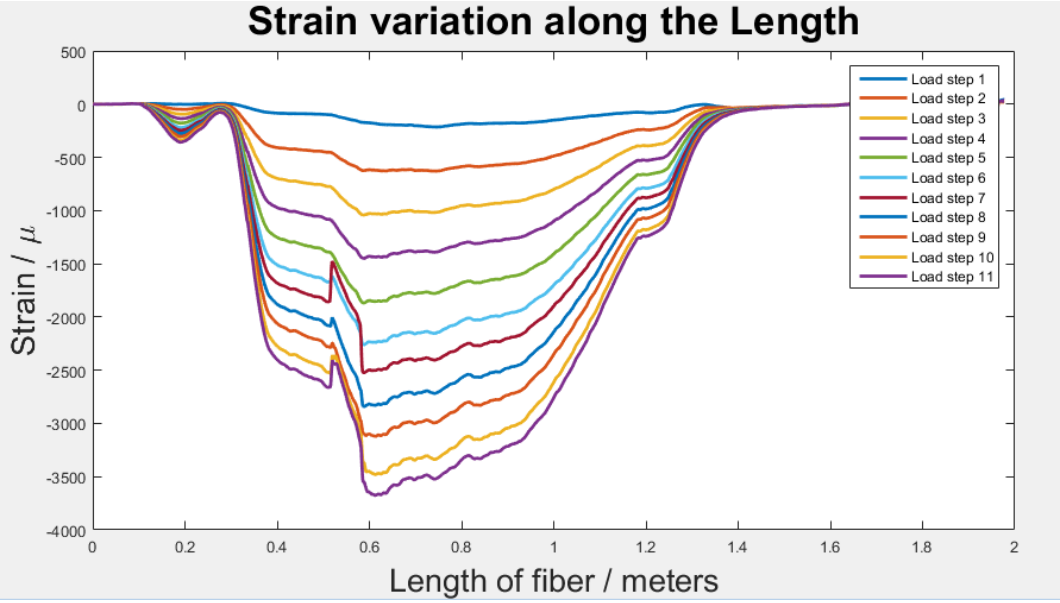


Figure 24: Sample span-wise strain data measured from optical strain measurement fibre

With the modal data available from the GVTs and the strains from the static tests, the next step is to perform a model-updating of the FE model. With the updated model a detailed comparison would be undertaken in comparing the experimental wind-tunnel and static test results with the original and updated models.

## 8 CONCLUSION

The work here presents the design, manufacturing and testing of three forward swept wings. The wings were optimized using the aeroelastic design framework developed in-house. The objective function in the optimization was to maximize tip deformation for two of the wings and to minimize mass for the third wing. Additionally, the deflection-maximized wings were subjected to a constraint on tip-twist such that under bending-upward displacement due to aerodynamic loads, the wings would have no positive nose-up twist. The wings were manufactured using conventional hand lay-up and vacuum bagging techniques.

Wind-tunnel tests were performed on the wings at the subsonic wind-tunnel (SWG) in Göttingen. Results comparing displacements, twists and lift forces between the experimental data and simulation data show good correlation. Importantly, the highly-flexible Wing 2 showed a maximum displacement of more than 18% of wing half-span with near-zero tip-twist as targeted.

The wind-tunnel experiments still showed some deviations in displacements resulting from idealizations in the FE model, its fidelity and deviations in the manufacturing. The next step to complete the loop is to update the FE model to match the physical structure. Toward this end, a GVT was performed using a Laser Doppler vibrometer and the mode shapes and natural frequencies were obtained. Additionally, Wing 2 was fabricated with an optical strain measurement fibre and static tests were conducted obtaining displacement and strain data. The processing of this data and subsequent model-updating will be the subject of future works.

## 9 BIBLIOGRAPHY

[1] Ghiasi, Hossein, et al. "Optimum stacking sequence design of composite materials Part I: Constant stiffness design." *Composite Structures* 90.1 (2009): 1-11.
[2] Ghiasi, Hossein, et al. "Optimum stacking sequence design of composite materials Part II: Variable stiffness design." *Composite Structures* 93.1 (2010): 1-13.
[3] Shirk, Michael H., Terrence J. Hertz, and Terrence A. Weisshaar. "Aeroelastic tailoring-theory, practice, and promise." *Journal of Aircraft* 23.1 (1986): 6-18.
[4] Vanderplaats, G. N., and T.A. Weisshaar. "Optimum design of composite structures." *International Journal for Numerical Methods in Engineering* 27.2 (1989): 437-448.
[5] Abdalla, M. M., R. De Breuker, and Z. Gürdal. "Aeroelastic tailoring of variable-stiffness slender wings for minimum compliance." *IFASD, Stockholm* (2007).
[6] Guo, Shijun J., J. R. Bannerjee, and C. W. Cheung. "The effect of laminate lay-up on the flutter speed of composite wings." *Proceedings of the Institution of Mechanical Engineers, Part G: Journal of Aerospace Engineering* 217.3 (2003): 115-122.
[7] Kameyama, Masaki, and Hisao Fukunaga. "Optimum design of composite plate wings for aeroelastic characteristics using lamination parameters." *Computers & structures* 85.3 (2007): 213-224.
[8] Guo, Shijun, Wenyuan Cheng, and Degang Cui. "Aeroelastic tailoring of composite wing structures by laminate layup optimization." *AIAA journal* 44.12 (2006): 3146-3150.
[9] Dillinger, J. K. S., et al. "Stiffness optimization of composite wings with aeroelastic constraints." *Journal of Aircraft* 50.4 (2013): 1159-1168.
[10] KRONE, JR, N. "Divergence elimination with advanced composites." *Aircraft Systems and Technology Meeting*. 1975.
[11] Weisshaar, Terrence A. "Aeroelastic tailoring of forward swept composite wings." *Journal of Aircraft* 18.8 (1981): 669-676.
[12] Librescu, Liviu, and SUROT THANGJITHAM. "Analytical studies on static aeroelastic behavior of forward-swept composite wing structures." *Journal of aircraft* 28.2 (1991): 151-157.
[13] Dillinger, Johannes, et al. "Static aeroelastic stiffness optimization and investigation of forward swept composite wings." *10th World Congress on Structural and Multidisciplinary Optimization*. 2013.
[14] Sherrer, V. C., T. J. Hertz, and M. H. Shirk. "Wind tunnel demonstration of aeroelastic tailoring applied to forward swept wings." *Journal of Aircraft* 18.11 (1981): 976-983.
[15] Meddaikar, Yasser M., et al. "Optimization, Manufacturing and Testing of a Composite Wing with Maximized Tip Deflection." *57th AIAA/ASCE/AHS/ASC Structures, Structural Dynamics, and Materials Conference*. 2016.
[16] Ritter, Markus, Johannes Dillinger, and Yasser M. Meddaikar. "Static and Dynamic Aeroelastic Validation of a Flexible Forward Swept Composite Wing." *58th AIAA/ASCE/AHS/ASC Structures, Structural Dynamics, and Materials Conference*. 2017.
[17] IJsselmuiden, Samuel Tsunduka. "Optimal design of variable stiffness composite structures using lamination parameters." *PhD diss., Delft University of Technology* (2011).
[18] IJsselmuiden, Samuel, et al. "Design of variable stiffness panels for maximum buckling load using lamination parameters." *49th AIAA/ASME/ASCE/AHS/ASC Structures, Structural Dynamics, and Materials Conference, 16th AIAA/ASME/AHS Adaptive Structures Conference, 10th AIAA Non-Deterministic Approaches Conference, 9th AIAA Gossamer Spacecraft Forum, 4th AIAA Multidisciplinary Design Optimization Specialists Conference*. 2008.

[19] Tsai, Stephen W., and Nicholas J. Pagano. *Invariant properties of composite materials*. No. AFML-TR-67-349. AIR FORCE MATERIALS LAB WRIGHT-PATTERSON AFB OHIO, 1968.
[20] Hahn, Hong T., and Stephen W. Tsai. *Introduction to composite materials*. CRC Press, 1980.
[21] Irisarri, F-X., et al. "Optimal design of laminated composite structures with ply drops using stacking sequence tables." *Composite Structures* 107 (2014): 559-569.
[22] Meddaikar, Yasser M., François-Xavier Irisarri, and Mostafa M. Abdalla. "Laminate optimization of blended composite structures using a modified Shepard's method and stacking sequence tables." *Structural and Multidisciplinary Optimization* (2016): 1-12.
[23] Zabinsky, Z. "Global optimization for composite structural design." *35th Structures, Structural Dynamics, and Materials Conference*. 1994.
[24] Haftka, Raphael T., and Zafer Gürdal. *Elements of structural optimization*. Vol. 11. Springer Science & Business Media, 2012.
[25] Khani, Ali, et al. "Design of variable stiffness panels for maximum strength using lamination parameters." *Composites Part B: Engineering* 42.3 (2011): 546-552.
[26] Abdalla, Mostafa, Zafer Gurdal, and Christos Kassapoglou. "Formulation of composite laminate robustness constraint in lamination parameters space." *50th AIAA/ASME/ASCE/AHS/ASC Structures, Structural Dynamics, and Materials Conference 17th AIAA/ASME/AHS Adaptive Structures Conference 11th AIAA No*. 2009.
[27] Schewe, G. "Force Measurements in Aeroelasticity Using Piezoelectric Multicomponent Transducers." *DGLR-Bericht 91-06* 91 (1991): 142-149.

## COPYRIGHT STATEMENT